Chemical Science

ROYAL SOCIETY OF CHEMISTRY

EDGE ARTICLE

View Article Online
View Journal

Check for updates

Cite this: DOI: 10.1039/d5sc05888k

All publication charges for this article have been paid for by the Royal Society of Chemistry

Open Access Article. Published on 17 November 2025. Downloaded on 12/2/2025 5:52:32 AM. This article is licensed under a Creative Commons Attribution-NonCommercial 3.0 Unported Licence.

The ultrastiff crystals of mucic (galactaric) acid

Durga Prasad Karothu, *[a] Ibrahim Tahir,[ab] Sanjit Manohar Majhi,[a] Ejaz Ahmed,[b] Luca Catalano,[c] Niamh T. Hickey,[de] James Weston,[f] Sarah Guerin[de] and Pančе Naumov *[abgh]

The upper limits of the stiffness of organic crystals, a newly established class of engineering materials, are an underexplored, yet very exciting domain of the material property space, because it could potentially provide ordered materials composed of light atoms with mechanical properties comparable to those of light metals and alloys. At present, however, the discovery of mechanically stiff and hard crystals is entirely serendipitous, since the relationships between the stiffness and crystal structure remain elusive. Here, guided by the very high density of the crystals of mucic (galactaric) acid, we investigated and report that this material is an ultrastiff organic crystal, with a Young's modulus obtained by nanoindentation on the (100)/($\bar{1}$00) pair of faces of $E = 50.25 \pm 1.55$ GPa and a hardness of $H = 2.81 \pm 0.15$ GPa ($n = 15$). This value of the modulus, which exceeds those of very stiff crystals such as α-glycine, tartaric acid and L-threonine, is corroborated by density functional theory (DFT) calculations, which provide an expectedly even higher value of $E = 68.5$ GPa. The measured moduli on the other two accessible faces are also above the higher approximate limit (25 GPa) of values that are common for organic crystals, with $E = 29.25 \pm 0.43$ GPa ($n = 70$) for the (001)/(00$\bar{1}$) faces and $E = 31.3 \pm 0.9$ GPa ($n = 15$) for the (010)/(0$\bar{1}$0) faces. Comparison with other organic crystals using material property plots not only underscores the unique combination of high stiffness and high density in this material, rooted in its extensive network of intermolecular hydrogen bonds, but also confirms that it has the highest-to-date measured surface stiffness among the organic crystals. This result is expected to guide the discovery of other extraordinarily stiff organic crystals that could be of interest as mechanically robust, lightweight materials.

Received 4th August 2025
Accepted 11th November 2025

DOI: 10.1039/d5sc05888k

rsc.li/chemical-science

Introduction

Higher-order natural biosystems combine the robustness of hard inorganic materials for mechanical support and softness and diffusion of soft matter for their physiological functions.[1–6] In a far analogy with this synergy, artificial construction materials such as metals and inorganics—now commonly produced on an industrial scale for their unmatched ability of mechanical reinforcement—are combined with softer materials and used for more intricate material designs in civil infrastructures.[7–10] The strength, ductility, fatigue resistance, flexibility, thermal stability, and hardness of specific material classes are also essential for applications in electronics, heavy machinery, and high-temperature devices.[11–14] More recently, however, well-established common materials, and especially chemically persistent polymers, are giving way to other, alternative, and less explored material classes. Small-molecule solids are one such long overlooked alternative.[15–20] Crystalline molecular solids appear somewhat paradoxical in their nature, because they are crystalline, yet they are also often mechanically soft. Being crystals, they are often intuitively expected to be hard and brittle;[19–21] this perception, however, is disparate with the recent reports of molecular crystals that undergo elastic or plastic deformation in response to external stress applied on specific crystallographic faces.[22–52] The compliance of these solids, composed of discrete molecules, is undoubtedly a result of the presence of intermolecular interactions, such as hydrogen bonding and other non-covalent interactions, which are energetically weakest in their structures. Because these solids are restricted by the low-energy interactions within natural limits of their stiffness, one of the challenges is the preparation of extremely stiff or hard organic crystals[20,53–57] that would be on par with the stiffness of soft solid

[a]Center for Smart Engineering Materials, New York University Abu Dhabi, PO Box 129188, Abu Dhabi, United Arab Emirates. E-mail: pance.naumov@nyu.edu; dpk3@nyu.edu

[b]Smart Materials Lab, New York University Abu Dhabi, PO Box 129188, Abu Dhabi, United Arab Emirates

[c]Dynamic Molecular Materials Laboratory, Dipartimento di Scienze della Vita, Università degli Studi di Modena e Reggio Emilia, 41125 Modena, Italy

[d]Department of Chemical Sciences, Bernal Institute, University of Limerick, V94 T9PX, Ireland

[e]SSPC, The Science Foundation Ireland Research Centre for Pharmaceuticals, University of Limerick, V94 T9PX, Ireland

[f]Core Technology Platforms, New York University Abu Dhabi, 129188 Abu Dhabi, United Arab Emirates

[g]Research Center for Environment and Materials, Macedonian Academy of Sciences and Arts, Bul. Krste Misirkov 2, MK-1000 Skopje, Macedonia

[h]Molecular Design Institute, Department of Chemistry, New York University, 100 Washington Square East, New York, NY 10003, USA

© 2025 The Author(s). Published by the Royal Society of Chemistry

Open Access Article. Published on 17 November 2025. Downloaded on 12/2/2025 5:52:32 AM.
This article is licensed under a Creative Commons Attribution-NonCommercial 3.0 Unported Licence.

metals or alloys.[53,54] In conjunction with other desirable properties—conductivity, optical translucency, non-linear interaction with light, and tunable emission—such materials could revolutionize the design of durable, flexible, and lightweight sensors, electronic devices, pharmaceuticals, and energetic materials.[53,58–62]

Molecular crystals that have high stiffness, as measured by their Young's moduli, are extremely rare. Examples of very stiff organic crystals include five amino acids or peptides with strong hydrogen bonds (α-glycine, γ-glycine, L-alanine, DL-serine, and glycylglycine),[54] pointing to the strength of hydrogen bonding as one of the contributing factors. A notable example of an ultrastiff crystal was reported in 2021 with L-threonine, a compound that has an extraordinarily high Young's modulus (40.95 ± 1.03 GPa) and hardness (1.98 ± 0.11 GPa) for an organic crystal.[53] The ongoing pursuit in the solid-state research community aimed at rationalizing the crystal stiffness with various structural characteristics such as bonding topology and strength benefits from systematic correlations between the mechanical properties and strength/density of strong intermolecular interactions.[15] In this study, we report that crystals of mucic acid (also known as galactaric acid, Fig. 1a), are a rare example of an ultrastiff crystal. The past interest in this material, which is widely used in the chemical, pharmaceutical, cosmetic, and food industries,[63] has been focused on its relevance to the synthesis of nylon, pyrone, and polyethylene furanoate.[64–66] In 1982, it was reported that its crystals have an unusually high density for an organic crystal of 1.790 g cm^{-3},[67] which exceeds the typical values for carbohydrate crystals (1.4–1.6 g cm^{-3}). Unlike pentaric acids such as D-mannaric acid and D-glucaric acid, mucic acid has very low solubility in water. Given the possible implications of the crystal's mechanical properties, these observations prompted us to characterize this material more extensively, and here we report that it is one of the stiffest organic crystalline materials reported to date.

Results and discussion

Since mucic acid exhibits very low solubility in most organic solvents, single crystals were grown using a modified version of the reported procedure.[67] Good-quality, colourless, elongated or block-shaped single crystals were obtained from an aqueous solution by slow evaporation at room temperature (Fig. 1b). The crystals have a relatively high melting point (m.p. 221 °C; see SI Fig. S1), and despite the fact that crystals of two habits were obtained, structural characterization confirmed that they were from the same polymorph (Fig. 1b).

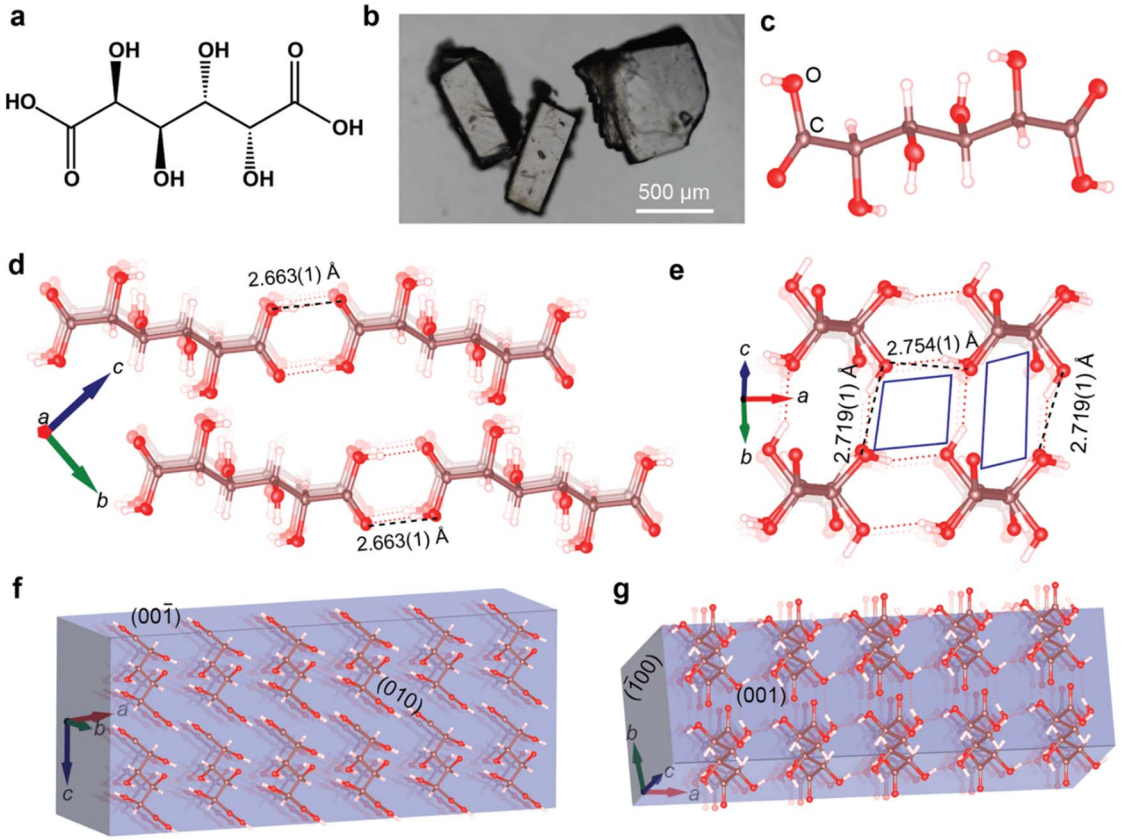

Fig. 1 Molecular and crystal structure details of mucic acid. (a) Molecular structure of mucic acid. (b) Optical images of crystals with two different habits. (c) ORTEP-style structure of the molecule in the crystal at the 50% probability level of the thermal ellipsoids. (d and e) Molecular packing diagram of end-to-end packing in the structure of mucic acid (the hydrogen bonds are shown as broken lines) (d), and the packing diagram showing the O–H···O hydrogen bonds forming parallelepiped-like patterns (e). (f and g) Extensive hydrogen bonding network in the crystal shown as viewed in two different directions. Note: the sketches in the plots in panels f and g are illustrations of the crystal shape and not the actual morphologies modelled from the crystal structure.

© 2025 The Author(s). Published by the Royal Society of Chemistry

Open Access Article. Published on 17 November 2025. Downloaded on 12/2/2025 5:52:32 AM.
This article is licensed under a Creative Commons Attribution-NonCommercial 3.0 Unported Licence.

Analysis of the crystal structure at room temperature (296 K) using single crystal X-ray diffraction (SI Table S1) showed that the crystals are triclinic, space group $P\bar{1}$ ($a = 4.9176(2)$ Å, $b = 5.8208(2)$ Å, $c = 6.8535(2)$ Å, $\alpha = 92.264(1)°$, $\beta = 94.208(1)°$ and $\gamma = 93.549(1)°$), with half a molecule in the asymmetric unit. The molecules interact with each other *via* strong hydrogen bonds involving all available functional groups, as shown in Fig. 1d–g. The hydroxyl groups are engaged in distinct parallelepiped-like hydrogen-bonded patterns with the adjacent molecules (Fig. 1e). The molecules form end-to-end chains by building on the typical carboxylic acid dimer motif across a center of symmetry (Fig. 1d). These molecular chains interact with each other *via* a network of strong hydrogen bonds between four hydroxyl groups.

The hydrogen bonding distance within the dimers is comparable to that of other carboxylic acids, with an H···O

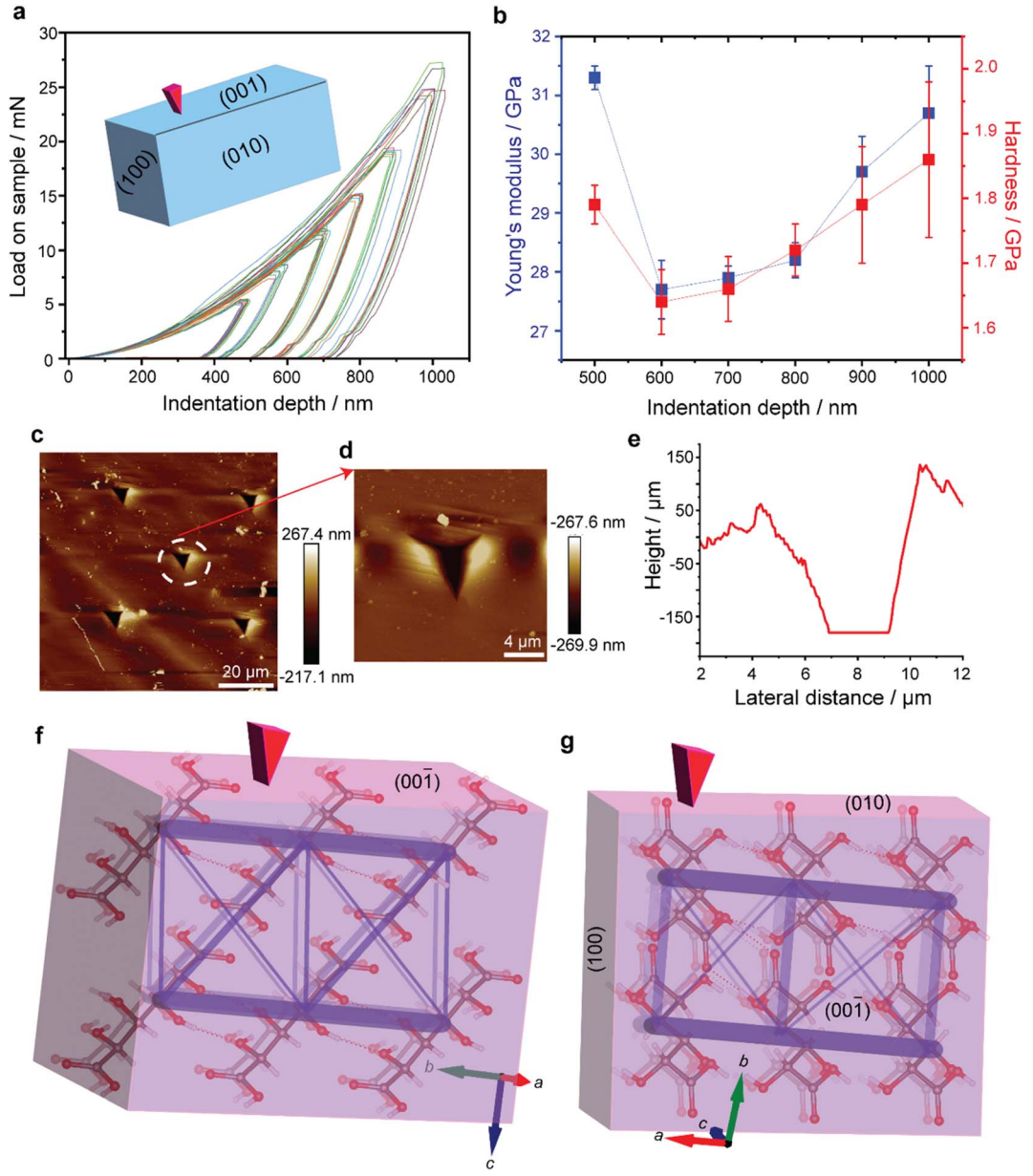

Fig. 2 Mechanical properties of mucic acid crystals. (a) Load–depth curves recorded from a mucic acid crystal on its (001)/(00$\bar{1}$) face at varying penetration depths. (b) Young's modulus (E) and hardness (H) based on the curves shown in (a). The error bars show the standard deviations that were calculated from at least 12 indents at each indentation depth. (c and d) AFM topography of the indent impressions. (c) Shows a topography of an indent after the completion of nanoindentation measurements and absence of material pileup. (e) Height profile of the indent shown in panel d. (f and g) Reconstructed energy framework analysis. The energy frameworks are illustrated as networks of blue cylinders linking the centers of mass of neighbouring molecules. The cylinder diameters correspond to the strength of interaction energies between the molecules. The interaction topologies are shown as viewed in two directions. The visualization of the outputs of the energy framework calculations has been reduced for clarity. Note: the sketches in panels f and g are illustrations of the crystal shape and not the actual crystal morphologies modelled from the crystal structure.

Open Access Article. Published on 17 November 2025. Downloaded on 12/2/2025 5:52:32 AM.
This article is licensed under a Creative Commons Attribution-NonCommercial 3.0 Unported Licence.

distance of 1.845(9) Å and a C···O distance of 2.663(1) Å. The structure suggests that the high density of mucic acid is a result of extensive hydrogen bonding and an exceptionally tight packing of hydrogen-bonded molecular chains (Fig. 1). We first utilized nanoindentation to assess the nanomechanical properties of the accessible faces of the crystal (Fig. 2 and SI Fig. S2). This method provided both stiffness (the degree to which an object resists elastic deformation under applied force) and hardness (the material's resistance to pressure or scratching by a sharp object). The crystal faces of mucic acid that were experimentally accessible for indentation were identified by the modelled Bravais–Friedel–Donnay–Harker (BFDH) morphology of the crystal based on the experimental crystal structure (SI Fig. S3). Fig. 2 shows the load-displacement curves at different indentation depths on the (001)/(00$\bar{1}$) faces, along with images of the impressions as inspected by atomic force microscopy (AFM). The elastic modulus (E) on the widely accessible (001)/(00$\bar{1}$) faces was found to be $E = 29.25 \pm 0.43$ GPa for depths between 500 and 1000 nm with a total of 70 indents (Fig. 2 and SI Fig. S4). On the (010)/(0$\bar{1}$0) faces, where the indentation was more difficult, the value was $E = 31.3 \pm 0.9$ GPa for 15 indents across the selected depth range (SI Fig. S2). These values surpass those of many organic molecular crystals, which typically range between 10 and 25 GPa, with only 8% of the reported organic crystals having values above the upper limit.[15] They are also significantly higher than the stiffness of materials considered to be stiff, which typically range between 16 and 23 GPa.[15,19] When compared to other stiff organic crystals, the Young's moduli on the (001)/(00$\bar{1}$) and (010)/(0$\bar{1}$0) faces of the crystals of mucic acid are only lower than those of α-glycine (44.00 GPa on

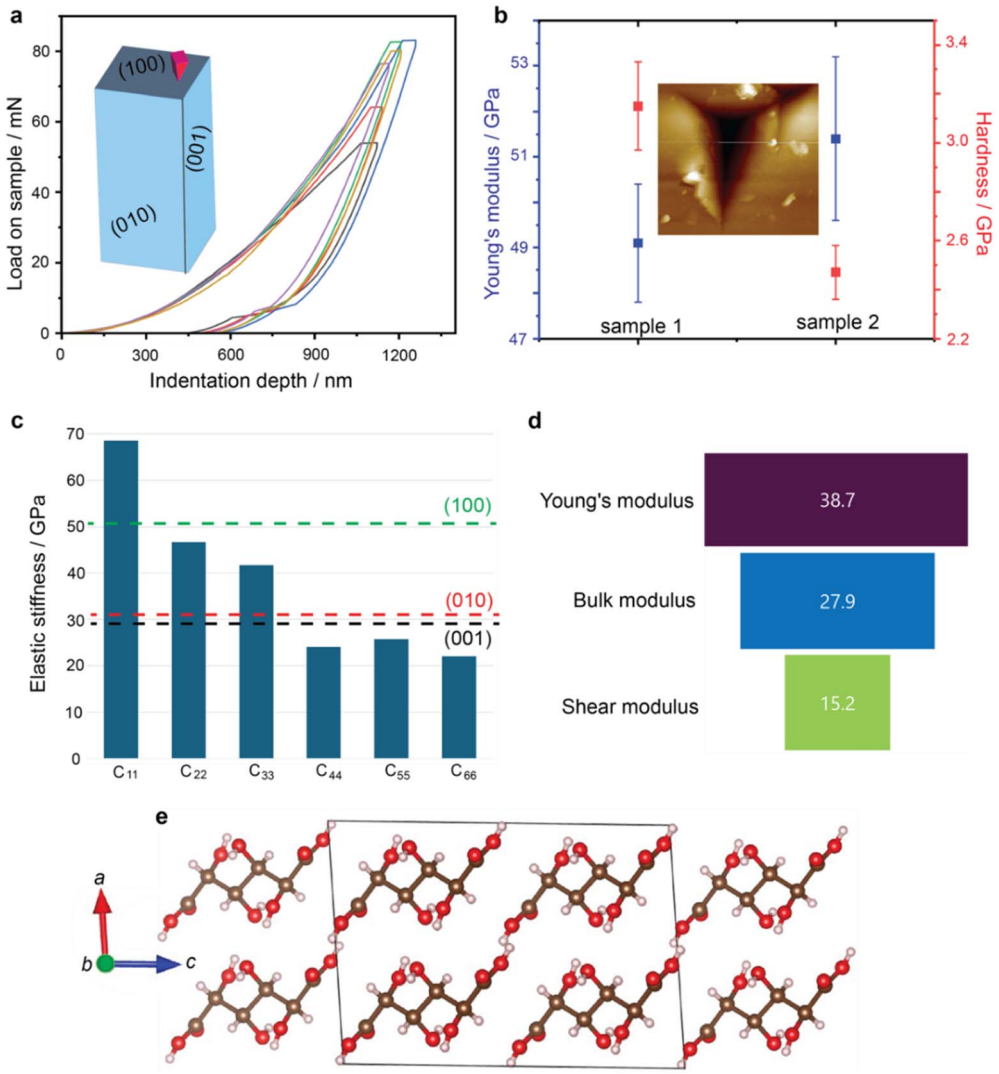

Fig. 3 Mechanical properties of mucic acid determined through experimental and computational techniques. (a) Load–depth curves recorded from a mucic acid crystal on its (100)/(1̄00) faces. (b) Young's modulus (E) and hardness (H) based on the curves shown in (a). The inset shows the AFM topography image of the indent impression, showing the absence of material pileup. (c) DFT-predicted elastic stiffness tensor coefficients for each c_{jj} component. The experimental values of the three moduli are shown as dashed lines. (d) Funnel chart of the theoretical bulk mechanical properties of mucic acid derived from DFT calculations (all values are in GPa). (e) DFT-optimized 2 × 1 × 2 unit cell of mucic acid. Note that the sketch in the plot is a representative illustration and not the actual modelled crystal morphology.

© 2025 The Author(s). Published by the Royal Society of Chemistry

Open Access Article. Published on 17 November 2025. Downloaded on 12/2/2025 5:52:32 AM.
This article is licensed under a Creative Commons Attribution-NonCommercial 3.0 Unported Licence.

the (001) face),[54] sucrose (35.96 GPa on the (001) face),[15] L-threonine (40.95 GPa on the (001) face),[53] and L-tartaric acid (43.34 GPa).[19] We note that the elastic moduli reported for β-succinic acid[68] and a few peptides[69] were not directly comparable to the values measured here due to the different method used to determine the Young's modulus of these compounds, which could systematically overestimate the actual values. The hardness (H) of the (001)/(00$\bar{1}$) and (010)/(0$\bar{1}$0) faces of mucic acid was determined to be $H = 1.74 \pm 0.06$ GPa and $H = 1.85 \pm 0.07$ GPa, respectively; these values are higher than those of many organic crystals (typically, between 0.1 to 1.0 GPa).[15,19] An attempt was then made to establish structure–mechanical property relationships by using energy framework analysis[17,70] to rationalize the observed exceptional mechanical properties of the mucic acid crystals. In Fig. 2f and g, the pairwise interaction energies in the crystal structure are depicted as cylinders connecting the individual molecules. The radii of these connecting cylinders are proportional to the relative strengths of the corresponding intermolecular interactions and strong interactions correspond to the thicker and larger cylinders. The analysis revealed that the extended intermolecular hydrogen bonding network results in a tightly packed crystal structure and relatively uniform distribution of energy among these intermolecular interactions, which could be the main factors that contribute to the high stiffness and hardness of the mucic acid crystals. Consistent with several previously reported examples,[17,71] the slightly higher Young's modulus observed on the (010)/(0$\bar{1}$0) face compared to that of the (001)/(00$\bar{1}$) face could be explained by the topology of intermolecular interactions, which point out to the interactions along the [010] crystallographic direction as being the strongest.

Notably, our energy framework analysis revealed that, among the three accessible crystallographic faces—(100), (010), and (001)—the intermolecular interaction topology (as depicted by the energy framework) shows the strongest interaction network along the [100] crystallographic direction, indicating that the most robust intermolecular interactions occur along this direction. This prompted us to determine the nanomechanical properties in that particular direction. Nanoindentation on this specific face, however, quickly proved to be challenging due to the very small available indentation area and the necessity to maintain the crystal in an upright position required to access that face. The sample tilting was minimized by affixing the crystal to the steel stage, which ultimately enabled us to indent that face. Fig. 3a shows the load-displacement curves at a selected indentation depth (1200 nm) on the (100)/($\bar{1}$00) face, and the inset of Fig. 3b shows an image of one of the impressions obtained by using AFM. Several indentations performed on several crystals returned values of the Young's modulus between 38 and 58 GPa. Most of these measurements and indent impressions were inspected after the indentation for any improper impressions and significant tilting, as the crystal had to remain in a straight position along its length (in some cases, very low values were obtained due to sample tilting). The elastic

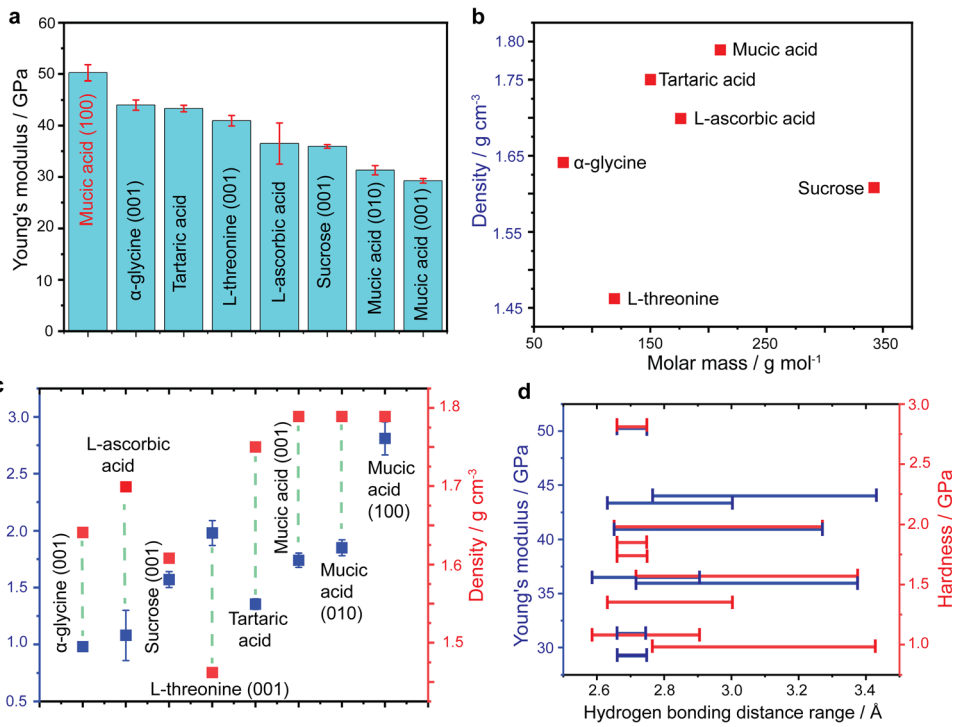

Fig. 4 Mechanical property correlation of mucic acid crystals and comparison with other stiff organic crystals. (a–c) Comparison of mucic acid with other organic crystalline materials having high Young's moduli (a), density and molar mass (b), and a plot of hardness (H) and density (c). (d) Plot of Young's modulus (E) and hardness (H) against the range of donor–acceptor distances extracted from the crystal structure of selected compounds including mucic acid. SI Table S3 provides the hydrogen bonding distance range of selected compounds (mucic acid, sucrose, tartaric acid, L-ascorbic acid, α-glycine and L-threonine).

Open Access Article. Published on 17 November 2025. Downloaded on 12/2/2025 5:52:32 AM.
This article is licensed under a Creative Commons Attribution-NonCommercial 3.0 Unported Licence.

modulus on the (100)/($\bar{1}$00) face was found to be $E = 50.25 \pm 1.55$ GPa for depths between 1000 and 1200 nm with a total of 15 indents (Fig. 3a, b and SI Fig. S5–S7). Fig. S6 and S7 show the indentation measurements performed on multiple crystals at varying penetration depths on (100)/($\bar{1}$00) face. It is noteworthy that, while slightly lower values were occasionally observed, nanoindentation measurements on multiple crystals—performed on the face perpendicular to the long axis—consistently demonstrated the exceptionally high stiffness of mucic acid crystals. These measurements are inherently challenging due to the crystals' anisotropic morphology, limited contact area (only a small fraction of the crystal face provides a sufficiently flat area for indentation, with the remainder exhibiting slope or surface irregularities) and potential for tilting or slippage during indentation. The obtained value is significantly higher than those reported for α-glycine (44.00 GPa on the (001) face),[54] sucrose (35.96 GPa on the (001) face),[15] L-threonine (40.95 GPa on the (001) face),[53] and L-tartaric acid (43.34 GPa),[19] and at present it is the highest stiffness reported for an organic crystal by nanoindentation. The hardness (H) of the (100)/($\bar{1}$00) face was determined to be $H = 2.81 \pm 0.15$ GPa.

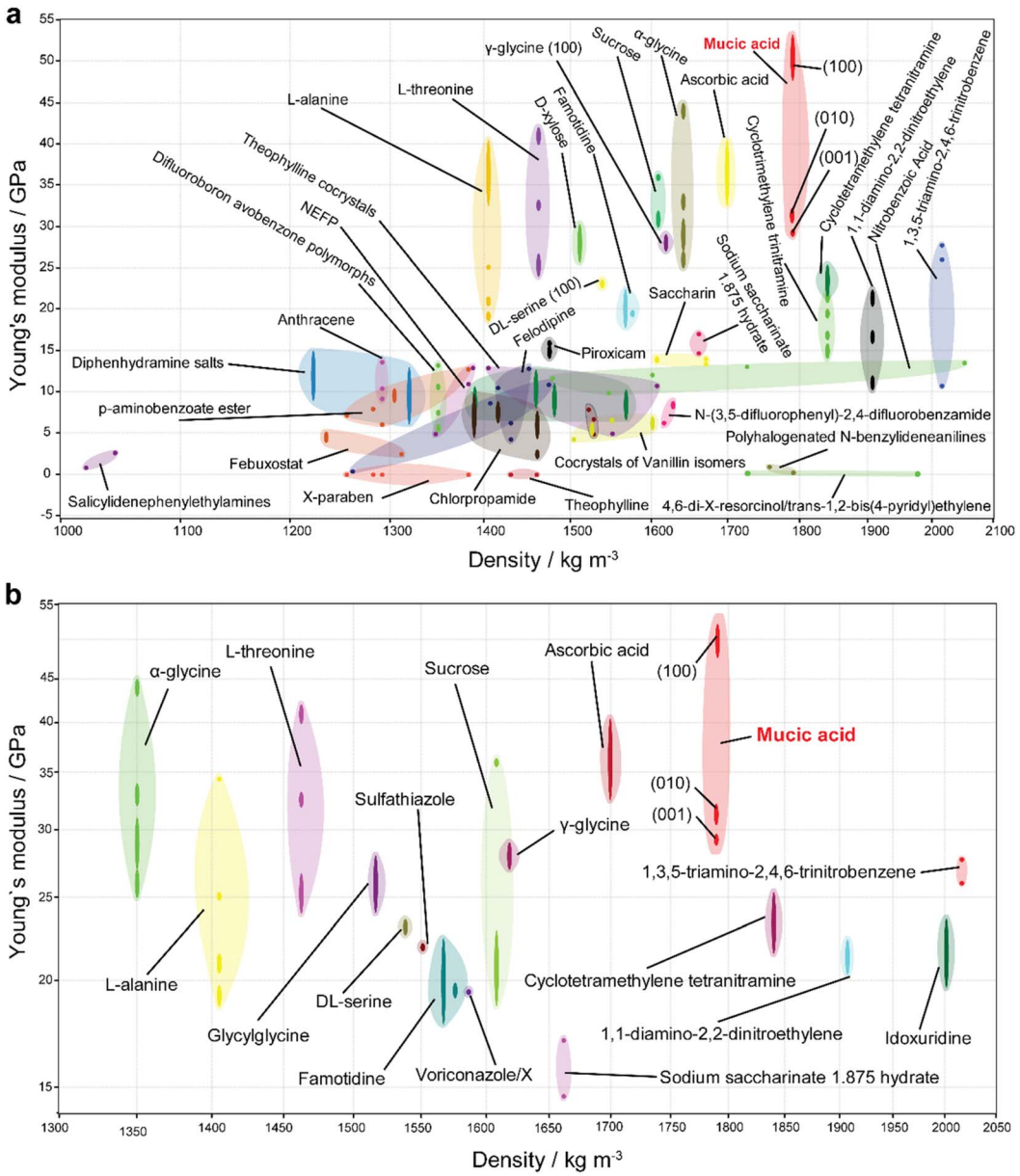

Fig. 5 Stiffness–density relationship of selected organic materials compared to mucic acid. (a) Ashby plot showing the relationship between Young's modulus (E) and density for a variety of organic crystalline materials. Mucic acid (highlighted in red) demonstrates higher Young's modulus (E) relative to many other organic crystals. (b) Selected area of the Ashby plot comparing the Young's modulus and density for materials with exceptionally high stiffness (over about 15 GPa). Mucic acid (highlighted in red) is shown to possess both high Young's modulus and high density.

© 2025 The Author(s). Published by the Royal Society of Chemistry

Open Access Article. Published on 17 November 2025. Downloaded on 12/2/2025 5:52:32 AM. This article is licensed under a Creative Commons Attribution-NonCommercial 3.0 Unported Licence.

Due to the experimental challenges and to confirm whether this experimentally observed mechanical stiffness is inherent to the crystal structure, we employed computational approaches to predict the mechanical properties of the (100)/($\bar{1}$00) faces, providing an independent assessment of the intrinsic stiffness of mucic acid crystals. The calculations were performed simultaneously for the remaining two pairs of faces, in order to corroborate the experimentally obtained values. Computational methods such as periodic density functional theory (DFT) calculations have been proven to be able to provide reliable predictions of mechanical properties, even for crystal facets that are experimentally inaccessible.[72,73] Fig. 3c and d shows the predicted c_{jj} values for mucic acid, corresponding to the anisotropic elastic stiffness in the direction j. The c_{22} and c_{33} values correspond to the directional stiffness on the (010) and (001) faces respectively, showing the same trend as experimental measurements. The calculated moduli, E = 46.7 and 41.7 GPa for the (010) and (001) faces, respectively, are higher than the experimental values of 31.3 and 29.25 GPa. This is to be expected as DFT values are calculated at absolute zero, and the high plane wave cutoff energy (SI Fig. S8) required for convergence results in shorter bond lengths and a denser crystal structure relative to room temperature. The highest predicted stiffness is that on the (100) face, with an exceptionally high value of E = 68.5 GPa. The derived bulk modulus of 27.9 GPa, the Young's modulus of 38.7 GPa, and the shear modulus of 15.2 GPa confirm that mucic acid is an exceptionally stiff crystal. Compared to other molecular crystals of similar size, the longitudinal tensor coefficient values (j = 1–3) are well above the average values,[16,54] with the predicted shear stiffness constants (j = 4–6), which vary between 22 and 26 GPa, being in the top 1% of molecular crystals in our recent high-throughput DFT screening.[74] The lowest of all the 36 tensor components (SI Table S2), some of which are equal in magnitude due to symmetry, is $c_{24} = c_{42}$ = 6 GPa.

Fig. 4 shows a comparison of the Young's modulus, hardness, and density between single crystals of mucic acid and other very stiff organic crystals: sucrose,[15] tartaric acid,[19] L-ascorbic acid,[15] and L-threonine.[53] As evident from Fig. 4b, the crystals of mucic acid have higher density compared to other stiff materials. Since the elastic modulus and hardness depend, among other factors, on the crystal density and direction of loading with respect to the strength of intermolecular interactions, this result prompted us to investigate the relationship between these properties and the hydrogen bonds. Even though intermolecular interactions determine the mechanical strength of the crystalline material to a significant extent, the stiffness and hardness cannot be rationalized exclusively by the presence of short intermolecular distances, as shown in Fig. 4d. We infer that, at a qualitative level, the unique molecular arrangement and strong intermolecular interactions in the structure of mucic acid contribute to the compactness of its structural packing and account for its exceptional mechanical properties.

On comparing Fig. 5a and b, it is evident that mucic acid occupies a distinct position in the mechanical property space of organic crystals. Fig. 5a illustrates a broad overview of the relationship between the Young's modulus and density across a wide range of organic materials, where mucic acid stands out due to its high stiffness relative to its high density. This position suggests that this material offers a unique balance between rigidity and weight, making it suitable for applications requiring lightweight, yet structurally robust materials. Fig. 5b narrows the focus to materials with higher Young's modulus values, further highlighting mucic acid's competitive stiffness in comparison to other high-modulus organic crystals. The clustering of mucic acid in Fig. 5b with materials of similar stiffness but varying densities underscores its potential as a strong candidate for engineering applications where high stiffness is desired without a proportional increase in density.

The comparison also emphasizes the exceptional combination of properties found in mucic acid, making it stand out among other well-known stiff organic crystals. The combined analysis of these plots reinforces the utility of this material in applications demanding both structural integrity and efficiency, and turns this and possibly other similar materials into candidates as lightweight organic substitutes for metals or alloys. A comparative summary of the Young's modulus of mucic acid with representative semicrystalline polymers, two-dimensional materials, and densely crosslinked polymers is provided in Table S4 (see the SI) to highlight its distinct mechanical characteristics relative to these material classes. We note that the values reported for mucic acid here approach those of pure aluminium ($E \approx$ 70 GPa) and are half that of copper ($E \approx$ 110 GPa). This places mucic acid among materials with significant stiffness, potentially offering advantages in applications requiring high mechanical strength while exhibiting a lower density compared to metals.

Conclusions

In summary, we have demonstrated that crystals of a simple organic compound, mucic acid, exhibit remarkable mechanical properties as assessed by the very high Young's modulus and hardness. These mechanical properties are superior to those of many other stiff organic materials. The high density and significantly high mechanical strength are rooted in a compact network of intermolecular interactions with extensive hydrogen bonding playing a crucial role in the mechanical robustness. The exceptional stiffness is also influenced by the structural topology and energy distribution of the intermolecular interactions. Upon analyzing the mechanical properties using nanoindentation, we observed that the (001)/(00$\bar{1}$), (010)/(0$\bar{1}$0) and (100)/($\bar{1}$00) faces of mucic acid crystals display some of the highest reported values for organic molecules. Analysis of the strength and orientation of interacting energies revealed relatively uniform distribution of interaction energies. Notably, the intermolecular interaction topology (energy frameworks) exhibits the strongest supramolecular columns along the [100] crystallographic direction, corroborated by DFT calculations of stiffness along the crystallographic a-axis. These factors collectively contribute to the exceptional mechanical properties of mucic acid single crystals. In the global mechanical property space, this material occupies a distinct position with its high stiffness and relatively high density. Its stiffness, comparable to

Open Access Article. Published on 17 November 2025. Downloaded on 12/2/2025 5:52:32 AM. This article is licensed under a Creative Commons Attribution-NonCommercial 3.0 Unported Licence.

that of other high-modulus organic crystals, makes it particularly well-suitable for applications requiring materials with both high mechanical strength and long-term durability.

Author contributions

D. P. K. and P. N. conceived the study. D. P. K. prepared the crystals and performed the experiments. D. P. K. performed crystallographic analysis, nanoindentation, energy framework analysis and thermal measurements. S. M. M., J. W. and D. P. K. performed AFM measurements. N. T. H. and S. G. performed computational analysis. D. P. K., I. T., E. A., and L. C. discussed the obtained results and contributed towards the preparation of Ashby plots. The article was written with contributions from D. P. K., P. N. and I. T. All authors have given approval to the final version of the article.

Conflicts of interest

There are no conflicts to declare.

Data availability

Data are available upon request from the authors.

CCDC 2378188 contains the supplementary crystallographic data for this article.[75]

Supplementary information (SI) is available. See DOI: https://doi.org/10.1039/d5sc05888k.

Acknowledgements

We thank Zainab Alhaddad for the help with the crystallization experiments. We thank New York University Abu Dhabi for the financial support of this work (project AD073). This research was partially carried out using the Core Technology Platform resources at New York University Abu Dhabi. This material is based upon studies supported by Tamkeen under NYUAD RRC Grant No. CG011. S. G. would like to acknowledge funding from Research Ireland under grant number 21/PATH-S/9737, ERC Starting Grant no. 101039636 and the Irish Centre for High-End Computing. N. T. H. was funded by Research Ireland award number 12/RC/2275_P2.

Notes and references

1 S. Coyle, C. Majidi, P. LeDuc and K. J. Hsia, *Ext. Mech. Lett.*, 2018, **22**, 51–59.
2 A. Miriyev, K. Stack and H. Lipson, *Nat. Commun.*, 2017, **8**, 596.
3 Y. Wang, S. E. Naleway and B. Wang, *Bioact. Mater.*, 2020, **5**, 745–757.
4 S. Li, H. Bai, R. F. Shepherd and H. Zhao, *Angew. Chem., Int. Ed.*, 2019, **58**, 11182–11204.
5 M. Ilami, H. Bagheri, R. Ahmed, E. O. Skowronek and H. Marvi, *Adv. Mater.*, 2021, **33**, 2003139.
6 M. C. Fernandes, J. Aizenberg, J. C. Weaver and K. Bertoldi, *Nat. Mater.*, 2021, **20**, 237–241.
7 P. A. Schweitzer, *Metallic materials: physical, mechanical, and corrosion properties*, CRC Press, 2003.
8 I. M. Ward and J. Sweeney, *Mechanical properties of solid polymers*, John Wiley & Sons, 2012.
9 J. J. Gilman, *Chemistry and physics of mechanical hardness*, John Wiley & Sons, 2009.
10 N. F. Mott, *Proc. Phys. Soc., London, Sect. B*, 1951, **64**, 729–742.
11 A. Pineau, A. A. Benzerga and T. Pardoen, *Acta Mater.*, 2016, **107**, 424–483.
12 C. D. Doyle, *Anal. Chem.*, 1961, **33**, 77–79.
13 N. A. N. Ouedraogo, Y. Chen, Y. Y. Xiao, Q. Meng, C. B. Han, H. Yan and Y. Zhang, *Nano Energy*, 2020, **67**, 104249.
14 D. Li, P. Liao, X. Shai, W. Huang, S. Liu, H. Li, Y. Shen and M. Wang, *RSC Adv.*, 2016, **6**, 89356–89366.
15 D. P. Karothu, J. Mahmoud Halabi, E. Ahmed, R. Ferreira, P. R. Spackman, M. A. Spackman and P. Naumov, *Angew. Chem., Int. Ed.*, 2022, **61**, e202113988.
16 P. R. Spackman, A. Grosjean, S. P. Thomas, D. P. Karothu, P. Naumov and M. A. Spackman, *Angew. Chem., Int. Ed.*, 2022, **61**, e202110716.
17 M. J. Turner, S. P. Thomas, M. W. Shi, D. Jayatilaka and M. A. Spackman, *Chem. Commun.*, 2015, **51**, 3735–3738.
18 G. Kaupp, J. Schmeyers and U. D. Hangen, *J. Phys. Org. Chem.*, 2002, **15**, 307–313.
19 C. Wang and C. C. Sun, *CrystEngComm*, 2020, **22**, 1149–1153.
20 S. Varughese, M. S. R. N. Kiran, U. Ramamurty and G. R. Desiraju, *Angew. Chem., Int. Ed.*, 2013, **52**, 2701–2712.
21 C. M. Reddy, G. R. Krishna and S. Ghosh, *CrystEngComm*, 2010, **12**, 2296–2314.
22 G. R. Krishna, R. Devarapalli, G. Lal and C. M. Reddy, *J. Am. Chem. Soc.*, 2016, **138**, 13561–13567.
23 E. Ahmed, D. P. Karothu and P. Naumov, *Angew. Chem., Int. Ed.*, 2018, **57**, 8837–8846.
24 P. Commins, D. P. Karothu and P. Naumov, *Angew. Chem., Int. Ed.*, 2019, **58**, 10052–10060.
25 P. Gupta, D. P. Karothu, E. Ahmed, P. Naumov and N. K. Nath, *Angew. Chem., Int. Ed.*, 2018, **57**, 8498–8502.
26 L. Catalano, D. P. Karothu, S. Schramm, E. Ahmed, R. Rezgui, T. J. Barber, A. Famulari and P. Naumov, *Angew. Chem., Int. Ed.*, 2018, **57**, 17254–17258.
27 D. P. Karothu, J. Weston, I. T. Desta and P. Naumov, *J. Am. Chem. Soc.*, 2016, **138**, 13298–13306.
28 M. Annadhasan, D. P. Karothu, R. Chinnasamy, L. Catalano, E. Ahmed, S. Ghosh, P. Naumov and R. Chandrasekar, *Angew. Chem., Int. Ed.*, 2020, **59**, 13821–13830.
29 W. M. Awad, D. W. Davies, D. Kitagawa, J. Mahmoud Halabi, M. B. Al-Handawi, I. Tahir, F. Tong, G. Campillo-Alvarado, A. G. Shtukenberg, T. Alkhidir, Y. Hagiwara, M. Almehairbi, L. Lan, S. Hasebe, D. P. Karothu, S. Mohamed, H. Koshima, S. Kobatake, Y. Diao, R. Chandrasekar, H. Zhang, C. C Sun, C. Bardeen, R. O. Al-Kaysi, B. Kahr and P. Naumov, *Chem. Soc. Rev.*, 2023, **52**, 3098–3169.
30 E. Ahmed, D. P. Karothu, M. Warren and P. Naumov, *Nat. Commun.*, 2019, **10**, 3723.

© 2025 The Author(s). Published by the Royal Society of Chemistry

Open Access Article. Published on 17 November 2025. Downloaded on 12/2/2025 5:52:32 AM. This article is licensed under a Creative Commons Attribution-NonCommercial 3.0 Unported Licence.

31 J. Ravi, A. V. Kumar, D. P. Karothu, M. Annadhasan, P. Naumov and R. Chandrasekar, *Adv. Funct. Mater.*, 2021, **31**, 2105415.
32 D. P. Karothu, G. Dushaq, E. Ahmed, L. Catalano, M. Rasras and P. Naumov, *Angew. Chem., Int. Ed.*, 2021, **60**, 26151–26157.
33 S. Hayashi, S. Yamamoto, D. Takeuchi, Y. Ie and K. Takagi, *Angew. Chem., Int. Ed.*, 2018, **57**, 17002–17008.
34 Z. Tang, X.-P. Sun, S.-D. Wang, X.-Y. Ji, Y. Li, Z.-S. Yao and J. Tao, *Sci. China Chem.*, 2022, **65**, 710–718.
35 M. Đaković, M. Borovina, M. Pisačić, C. B. Aakeröy, Ž. Soldin, B.-M. Kukovec and I. Kodrin, *Angew. Chem., Int. Ed.*, 2018, **57**, 14801–14805.
36 A. J. Thompson, A. I. Chamorro Orué, A. Jayamohanan Nair, J. R. Price, J. McMurtrie and J. K. Clegg, *Chem. Soc. Rev.*, 2021, **50**, 11725–11740.
37 A. Worthy, A. Grosjean, M. C. Pfrunder, Y. Xu, C. Yan, G. Edwards, J. K. Clegg and J. C. McMurtrie, *Nat. Chem.*, 2018, **10**, 65–69.
38 P. Gupta, S. Allu, D. P. Karothu, T. Panda and N. K. Nath, *Cryst. Growth Des.*, 2021, **21**, 1931–1938.
39 P. Gupta, S. A. Rather, B. K. Saha, T. Panda, D. P. Karothu and N. K. Nath, *Cryst. Growth Des.*, 2020, **20**, 2847–2852.
40 P. Naumov, S. Chizhik, M. K. Panda, N. K. Nath and E. Boldyreva, *Chem. Rev.*, 2015, **115**, 12440–12490.
41 P. Naumov, D. P. Karothu, E. Ahmed, L. Catalano, P. Commins, J. Mahmoud Halabi, M. B. Al-Handawi and L. Li, *J. Am. Chem. Soc.*, 2020, **142**, 13256–13272.
42 Y. Chen, Z. Chang, J. Zhang and J. Gong, *Angew. Chem., Int. Ed.*, 2021, **60**, 22424–22431.
43 S. Kusumoto, Y. Kim and S. Hayami, *Coord. Chem. Rev.*, 2023, **475**, 214890.
44 C. M. Reddy, R. C. Gundakaram, S. Basavoju, M. T. Kirchner, K. A. Padmanabhan and G. R. Desiraju, *Chem. Commun.*, 2005, 3945–3947.
45 S. Ghosh and C. M. Reddy, *Angew. Chem., Int. Ed.*, 2012, **51**, 10319–10323.
46 T. Seki, N. Hoshino, Y. Suzuki and S. Hayashi, *CrystEngComm*, 2021, **23**, 5686–5696.
47 K. Wang, M. K. Mishra and C. C. Sun, *Chem. Mater.*, 2019, **31**, 1794–1799.
48 H. Liu, K. Ye, Z. Zhang and H. Zhang, *Angew. Chem., Int. Ed.*, 2019, **58**, 19081–19086.
49 X. Chu, Z. Lu, B. Tang, B. Liu, K. Ye and H. Zhang, *J. Phys. Chem. Lett.*, 2020, **11**, 5433–5438.
50 S. Tang, K. Ye and H. Zhang, *Angew. Chem., Int. Ed.*, 2022, **61**, e202210128.
51 K. Chen, J. Wang, W. Wu, H. Shan, H. Zhao, N. Wang, T. Wang, X. Huang and H. Hao, *Dyes Pigm.*, 2023, **219**, 111536.
52 M. K. Panda, K. B. Pal, G. Raj, R. Jana, T. Moriwaki, G. D. Mukherjee, B. Mukhopadhyay and P. Naumov, *Cryst. Growth Des.*, 2017, **17**, 1759–1765.
53 D. P. Karothu, G. Dushaq, E. Ahmed, L. Catalano, S. Polavaram, R. Ferreira, L. Li, S. Mohamed, M. Rasras and P. Naumov, *Nat. Commun.*, 2021, **12**, 1326.
54 I. Azuri, E. Meirzadeh, D. Ehre, S. R. Cohen, A. M. Rappe, M. Lahav, I. Lubomirsky and L. Kronik, *Angew. Chem., Int. Ed.*, 2015, **54**, 13566–13570.
55 F. Liu, D. E. Hooks, N. Li, N. A. Mara and J. A. Swift, *Chem. Mater.*, 2018, **30**, 3798–3805.
56 W. C. Oliver and G. M. Pharr, *J. Mater. Res.*, 2004, **19**, 3–20.
57 U. Ramamurty and J. Jang, *CrystEngComm*, 2014, **16**, 12–23.
58 J. D. Bauer, E. Haussühl, B. Winkler, D. Arbeck, V. Milman and S. Robertson, *Cryst. Growth Des.*, 2010, **10**, 3132–3140.
59 K. J. Ramos, D. E. Hooks and D. F. Bahr, *Philos. Mag.*, 2009, **89**, 2381–2402.
60 K. J. Ramos, D. F. Bahr and D. E. Hooks, *Philos. Mag.*, 2011, **91**, 1276–1285.
61 A. M. Reilly and A. Tkatchenko, *Phys. Rev. Lett.*, 2014, **113**, 055701.
62 S. Karki, T. Friščić, L. Fabian, P. R. Laity, G. M. Day and W. Jones, *Adv. Mater.*, 2009, **21**, 3905–3909.
63 D. E. Kiely, L. Chen and T. H. Lin, *J. Am. Chem. Soc.*, 1994, **116**, 571–578.
64 S. Song, J. G. Zhang, G. Gozaydin and N. Yan, *Angew. Chem., Int. Ed.*, 2019, **58**, 4934–4937.
65 G. Leonardi, J. Li, G. I. C. Righetti, A. M. Truscello, C. Gambarotti, G. Terraneo, A. Citterio and R. Sebastiano, *Eur. J. Org Chem.*, 2020, **2020**, 241–251.
66 N. van Strien, S. Rautiainen, M. Asikainen, D. A. Thomas, J. Linnekoski, K. Niemelä and A. Harlin, *Green Chem.*, 2020, **22**, 8271–8277.
67 G. A. Jeffrey and R. A. Wood, *Carbohydr. Res.*, 1982, **108**, 205–211.
68 S. Haussühl, *Z. Krist.*, 1995, **210**, 903–904.
69 S. Bera, S. Mondal, B. Xue, L. J. W. Shimon, Y. Cao and E. Gazit, *Nat. Mater.*, 2019, **18**, 503–509.
70 P. R. Spackman, M. J. Turner, J. J. McKinnon, S. K. Wolff, D. J. Grimwood, D. Jayatilaka and M. A. Spackman, *J. Appl. Crystallogr.*, 2021, **54**, 1006–1011.
71 S. P. Thomas, M. W. Shi, G. A. Koutsantonis, D. Jayatilaka, A. J. Edwards and M. A. Spackman, *Angew. Chem., Int. Ed.*, 2017, **56**, 8468–8472.
72 E. Kiely, R. Zwane, R. Fox, A. M. Reilly and S. Guerin, *CrystEngComm*, 2021, **23**, 5697–5710.
73 J. D. Evans and F.-X. Coudert, *Chem. Mater.*, 2017, **29**, 7833–7839.
74 S. Vishnoi, G. Kumari, R. Guest, P.-A. Cazade and S. Guerin, *Angew. Chem., Int. Ed.*, 2025, **64**, e202501232.
75 CCDC 2378188: Experimental Crystal Structure Determination, 2025, DOI: 10.5517/ccdc.csd.cc2ktprv.